JOURNAL OF COMPUTATIONAL PHYSICS 110, 257–273 (1994)

The Spectral Viscosity Method Applied to Simulation of Waves in a Stratified Atmosphere

ØYVIND ANDREASSEN, IVAR LIE, AND CARL ERIK WASBERG

Norwegian Defence Research Establishment, P.O. Box 25, 2007 Kjeller, Norway

Received December 16, 1992

A spectral collocation method is used to solve an atmospheric gravity wave simulation problem, modelled by the non-linear, inviscid, two-dimensional Euler equations including gravity. The non-linear transfer of energy to higher frequencies will destroy the long-time calculations if no energy dissipation mechanism is introduced in the numerical method. The spectral viscosity method is applied for this purpose, and we discuss implementation aspects, effects on the resulting system of ordinary differential equations, tuning of parameters, and evaluation of results. An implementation is found that works well also for larger simulations, and guidelines for the application of the method are given.

1. INTRODUCTION

Spectral methods have been highly successful in simulations of fluid flow where high accuracy is required. Among the reasons for this success is the non-dissipative and non-dispersive character of the methods, which makes it possible to do calculations over large scales and long times and still retain high accuracy. However, the absence of numerical dissipation also introduces problems, which is the issue of this paper.

We consider an atmosphere modelled by the inviscid, compressible Euler equations with a gravity term included. The density and pressure of the steady-state solution decay exponentially with the height, and this stratification gives rise to increasing amplitudes of gravity waves and sound waves with height. Gravity waves are believed to play an important role in the energetics of the atmosphere [8]. The system of partial differential equations expressing the motion in an ideal fluid is non-linear and hyperbolic, a combination which often introduces shocks in the solution. In the atmosphere, the sound waves will in some special situations appear as shock waves while the gravity waves will develop vortices and turbulent structures as the non-linearities become important. The situation studied in this paper does not involve shocks, but the non-linear terms in the equations will transfer energy to higher frequencies. The natural dissipation scale in this case is much smaller than the typical length scale of the phenomena of interest, so it is presently beyond reach to represent both scales in a calculation.

In a numerical simulation using a spectral method, the energy that is transferred to the highest frequencies will, unless it is taken care of in some way, be reflected back to the lower frequencies and destroy even the large-scale structures of the solution. This problem can be approached by trying to model the effects of the physical processes acting on smaller scales than those represented in the simulation (e.g., [6, 17, 18]), or by trying to solve the original hyperbolic equations as accurately as possible (e.g., [3, 22]).

This paper contains an application of the spectral viscosity (SV) method to the simulation of gravity waves. The SV method was introduced by Tadmor in [22] and is a way to stabilize spectral solutions of non-linear hyperbolic PDEs by adding small artificial, frequency-dependent viscosity terms to the equations. We hope that the results and conclusions presented in the present paper will be valuable in applications of the SV method.

The basic numerical method is a two-dimensional spectral collocation method [4] with a Fourier expansion in the horizontal direction, which is assumed periodic, and a Chebyshev expansion in the vertical direction. The SV method with Chebyshev basis functions has previously been less studied than with Fourier and Legendre expansions. The computational domain is divided into two subdomains using characteristic interface conditions to match the solutions and open boundary conditions based on characteristics which are applied at the upper and lower boundaries [24]. The solution is advanced in time by a second-order Runge–Kutta method with variable time-steps, which also serves as an important tool to monitor the calculations and to aid the tuning of spectral viscosity parameters.

The paper is organized as follows. The background for the physical model and the processes acting in the situation that is used as a test case in this paper are presented in Section 2. The basic numerical method is outlined in Section 3, and the spectral viscosity method is described

0021-9991/94 $6.00

in Section 4. Section 5 discusses the system of ordinary differential equations resulting from the spectral discretization in space, suitable solution methods, and the effect of spectral viscosity. Results from numerical calculations, together with discussions of parameter tuning and other questions encountered in the application of the SV method are presented in Section 6, while Section 7 contains the conclusions.

2. THE PHYSICAL MODEL

The physical model problem which we will use as a test case for the numerical algorithms is a strongly non-linear gravity wave/wind shear interaction problem [7]. Consider a stratified fluid containing a horizontal wind with a vertically increasing speed such that at a certain height h_c, the velocity is V_c. Consider a gravity wave with horizontal phase speed $V_p = V_c$. An observer moving with the fluid at level h_c will see a stationary medium. As described in detail in [7] the energy and momentum of the wave is piled up below the level $h = h_c$ called the critical level. The speed V_c is called the critical speed. The wind shear acts as a filter blocking the waves, with neglectable transmission and reflection of energy upwards and downwards. As the energy and momentum density increases, non-linear effects become increasingly more important. The amplitude and the shear of the wave field increases until instabilities set in and cause the wave field to break up. The ultimate state of development of this process is turbulence.

The physical evolution of turbulence as a result of gravity wave breaking is correctly described only in three dimensions [1], but for experiments with the numerical method it is sufficient to consider a two-dimensional model. The model presented here consists of the equations for conservation of mass, momentum, and energy describing non-linear dynamics in an inviscid, compressible, plane parallel, stratified fluid, where the motion is assumed to be adiabatic:

$$\frac{\partial \rho}{\partial t} + \nabla \cdot (\rho \mathbf{v}) = 0,$$

$$\rho \frac{d\mathbf{v}}{dt} = -\nabla p + \rho \mathbf{g} + \mathbf{F}, \tag{1}$$

$$\frac{dp}{dt} + \gamma p \nabla \cdot \mathbf{v} = 0,$$

Here $\mathbf{v}$ is the velocity, ρ is the density, p is the pressure, $\mathbf{g}$ is the acceleration of gravity ($|\mathbf{g}| = g$), and γ is the ratio of specific heats. We have non-dimensionalized all variables with respect to the density scale height H, the sound-speed c_s, with $c_s^2 = \gamma g H$, a time scale H/c_s, and reference temperature T_0, density ρ_0, and pressure p_0 all computed at the lower boundary of the model. With these choices, the isothermal Brunt-Väisälä frequency squared become $N^2 = (\gamma - 1)/\gamma$.

The pressure and density are related to temperature through the equation of state for an ideal gas, $p = \rho RT$, and we use the potential temperature $\theta = T(p_0/p)^{R/c_p}$ as a tracer of fluid motion. The reason that this can be used is that for adiabatic motion, the potential temperature is preserved for each fluid element. The potential temperature is constant for an atmosphere in adiabatic equilibrium, for which the gradient $dT/dz = -g/c_p = \alpha$. When the gradient becomes super-adiabatic ($dT/dz < \alpha$), the atmosphere becomes convectively unstable and $d\theta/dz < 0$. When a gravity wave breaks, some local patches of its field may become super-adiabatic. Then $d\theta/dz$ changes value to negative in these patches and this is seen as "overturning" of the isolines of θ, as seen in Fig. 3. The isolines of θ outlines the phaselines of the material displacement in the gravity wave field as long as the motion is adiabatic.

Cartesian coordinates (x, z) are used, with the x axis pointing along the horizontal direction while z points vertically opposite to the direction of $\mathbf{g}$. We consider a computational domain that is four scale heights wind and five and a half scale heights high.

To excite the waves, a force $\mathbf{F} = f(x, z, t)\,\hat{\mathbf{z}}$ is smoothly turned on, held at a constant amplitude and smoothly turned down to zero. This is done to avoid transients in the solution. The function f is given by the expression

$$f(x,z,t) = \begin{cases} f_0 \sqrt{t/10.0}\exp\{-(z-\delta)^2/\sigma^2\}\sin\{\omega t - kx\}, \\ \qquad 0 \leqslant t \leqslant 10.0, \\ f_0 \exp\{-(z-\delta)^2/\sigma^2\}\sin\{\omega t - kx\}, \\ \qquad 10.0 < t \leqslant 50.0, \\ f_0 \sqrt{(50.0-t)/10.0}\exp\{-(z-\delta)^2/\sigma^2\} \\ \qquad \times \sin\{\omega t - kx\}, \qquad 50.0 < t \leqslant 60.0, \\ 0, \qquad 60.0 < t. \end{cases}$$

Here $f_0 = 0.02$ is the forcing amplitude, $\delta = 3$ is the height from the lower boundary of maximum force, and $\sigma = 0.5$ expresses the width of the force. The frequency is $\omega = \pi/10$, which is well below N to make sure that the waves are internal gravity waves, and the wavenumber is $k = \pi/2$, making the horizontal phase speed $V_p = 0.2$.

As the initial condition we assume a horizontal mean motion

$$u(t=0) = U_0(z) = \begin{cases} 0, & 0 \leqslant z \leqslant 4, \\ 0.2(1 + \cos\{\pi(\frac{1}{4} + (\frac{3}{4})(5.5 - z)/1.5)\}), \\ 4 < z \leqslant 5.5. \end{cases}$$

This function is selected such that the velocity $U_0(z)$ at $z = 5$ is equal to the horizontal phase speed V_p of the generated waves to form a critical level. The instability and the region

of development of the non-linear phenomena is then positioned well within the boundaries of the domain. It is assumed that the fluid is initially isothermal and in hydrostatical equilibrium described by

$$\frac{\partial p}{\partial z} = -\rho g, \quad \text{i.e.,} \quad \rho(z) = \rho_0 e^{-z}, \quad p(z) = g\rho_0 e^{-z}. \tag{2}$$

The strong non-linear effects occurring around the critical level lead to a fast cascade of energy from large to small scales. In nature the cascade continues until a viscous scale is reached and the energy is dissipated. When modelling the atmosphere and ocean, the variety of scales from the largest, where energy is injected (buoyancy scales, which are the scales of internal waves) down to the smallest scales (viscous scales), where the energy is dissipated, is very large. Therefore we have to limit the treatment to scales which can be handled and hopefully are of importance for the problem. That is, to the buoyancy scale and at best to some of the inertial scale, where the turbulence is generated.

Equations (1) could contain dissipation terms $\nabla(\nu \cdot \nabla \mathbf{v})$ in the momentum equation and $\nabla(\kappa \cdot \nabla T)$ in the energy equation: ν is the kinematic viscosity coefficient, κ is the thermal diffusion coefficient, and the ratio of these is the Prandtl number, $\sigma = \nu/\kappa$, which is ≈ 0.7 for the earth's atmosphere [13]. As explained above, the physical values of ν and κ as measured for air are too small to make any impact on the numerical calculations. If larger values are assigned in order to stabilize the numerical scheme, we proceed as follows to retain a sensible "numerical" Prandtl number: The non-linear effects dominate at a height of five from the lower boundary of the model, and the requirement of damping is therefore strongest at this height. All variables are scaled according to values at the lower boundary of the model. The diffusion equations $u_t \approx \nu \nabla^2 u$ and $p_t \approx \kappa \nabla^2 T$ determines the magnitude of the damping. For gravity waves with small amplitudes we can write $T \approx 1/\gamma + \delta(1 - 1/\gamma)\, e^{z/2}$, and the pressure perturbation goes like $\delta e^{-z/2}$. To give a uniform thermal damping, κ should vary like $\kappa(z) = \kappa_0 e^{-z}$. From the diffusion equation for velocity it is apparent that the viscosity is scaled to be the same at all heights. To scale the "numerical" Prandtl number to around 0.7 at the lower boundary, we should have $\nu(z=5)/\kappa(z=5) = \nu_0/\kappa_0 e^{-5} \approx 0.7e^5 \approx 104$. If a constant value of κ is used, the ratio ν/κ should therefore be around 100 to obtain a good balance of the dissipation terms at $z \sim 5$.

3. THE NUMERICAL METHOD

We use a spectral collocation method [4], where the numerical solution is sought in the function space $V_{M,N} = S_M \otimes \mathbb{P}_N$, where $S_M = \text{span}\{e^{imx} \mid -M/2 \leqslant m \leqslant M/2 - 1\}$ and $\mathbb{P}_N = \text{span}\{x^n \mid 0 \leqslant m \leqslant N\}$. A function in $V_{M,N}$ is denoted by a superscript V and can be represented by its values at the collocation points

$$\begin{aligned} x_k &= 2k\pi/M, \qquad 0 \leqslant k < M, \\ z_l &= \cos(l\pi/N), \qquad 0 \leqslant l \leqslant N, \end{aligned} \tag{3}$$

given by the double sum

$$u^V(x_k, z_l) = \sum_{m=-M/2}^{M/2-1} \sum_{n=0}^{N} a_{mn} e^{imx_k} T_n(z_l), \tag{4}$$

where $T_n(z) = \cos(n \arccos(z))$ is the Chebyshev polynomial of order n.

The physical situation described in the previous section suggests this use of periodic basis functions in the horizontal (x) direction, because the background wind profile is constant in x, and the generated gravity waves can naturally be considered periodic. The vertical (z) direction is aperiodic due to the gravity, therefore the Chebyshev basis is chosen. Chebyshev polynomials are preferred to Legendre or other sets of orthogonal polynomials because of the possibility of using fast Fourier transforms in the implementation.

The numerical approximations of the physical variables are denoted ρ^V, u^V, v^V, and p^V, and the equations to be solved can be written in vector form as

$$\frac{\partial U^V}{\partial t} + A\frac{\partial U^V}{\partial x} + B\frac{\partial U^V}{\partial z} = b, \tag{5}$$

where

$$A = \begin{pmatrix} u^V & \rho^V & 0 & 0 \\ 0 & u^V & 0 & 1/\rho^V \\ 0 & 0 & u^V & 0 \\ 0 & \gamma p^V & 0 & u^V \end{pmatrix},$$

$$B = \begin{pmatrix} u^V & 0 & \rho^V & 0 \\ 0 & v^V & 0 & 0 \\ 0 & 0 & v^V & 1/\gamma^V \\ 0 & 0 & \gamma p^V & v^V \end{pmatrix},$$

$$U^V = (\rho^V, u^V, v^V, p^V)^{\mathrm{T}}, \qquad b = (0, 0, -g, 0)^{\mathrm{T}},$$

with given initial conditions, and boundary conditions described below at the upper and lower boundaries. The space derivatives in (5) are calculated by exact differentiation of the components of U^V, and when we require (5) to be satisfied at the collocation points (3), (5) define a coupled system of $4M(N+1)$ ordinary differential equations for the grid point values (or, equivalently, for the spectral coefficients). The solution of this ODE-set is discussed in Section 5.

To reduce the amount of work needed to calculate the space derivatives, the computational area is split into two domains, one above the other. This domain decomposition permits the use of higher resolution in the area around the critical level than in the more regular areas of the flow. The same effect could be achieved by a coordinate transformation, but the decomposition is computationally more efficient. This is because the calculation of each of the spatial derivatives in the vertical direction requires $\mathcal{O}(N \log N)$ operations even with FFT (and $\mathcal{O}(N^2)$ with matrix multiplication), but also because the stability restriction on the time-steps is of order $1/N^2$ when N is the number of collocation points in the Chebyshev direction. Of course, the resolution in both domains must be sufficient to resolve the important features of the solution. We know that two grid points per wavelength are needed in the periodic direction, and if the Chebyshev direction contains n wavelengths the number of grid points should be at least πn [9]. The next section discusses how to avoid underresolved calculations, and as long as this is achieved we follow the discussion in [4] and neglect aliasing errors.

At the domain interface we consider a quasi-one-dimensional linearization of Eqs. (1), where horizontal derivatives are ignored and the coefficients are frozen at each time-step. This system of equations is on the form

$$U_t + \hat{B} U_z = b,$$

where $\hat{B}$ is the matrix of the frozen coefficients. This system has the following eigenvalues $\{\lambda_i\}_{i=1}^4$ and characteristic variables $\{\psi_i\}_{i=1}^4$:

$$\lambda_1 = \hat{v} - \hat{a}, \qquad \lambda_2 = \lambda_3 = \hat{v}, \qquad \lambda_4 = \hat{v} + \hat{a}, \tag{6}$$

$$\begin{aligned} \psi_1 &= -\hat{\rho}\hat{a}v + p, \qquad \psi_2 = u, \\ \psi_3 &= \rho - p/\hat{a}^2, \qquad \psi_4 = \hat{\rho}\hat{a}v + p. \end{aligned} \tag{7}$$

The hats indicate values at the previous time-step, and $\hat{a} = \sqrt{\gamma \hat{p}/\hat{\rho}}$ is the sound-speed at the previous time-step. After each time-step of the ODE-integration, a boundary correction procedure is invoked, where the characteristic variables are calculated using values from the "upstream" domain (determined by the sign of the corresponding eigenvalues). Equation (7) then gives four equations for the determination of the four physical variables at each boundary point.

The same principle is used at the upper and lower boundaries. We want these boundaries to be open, such that waves approaching the boundaries will leave the computational domain without reflections. As discussed in [24], incoming "fast" characteristics (corresponding to the eigenvalues λ_1 or λ_4) are given their hydrostatic background values from (2). "Slow" incoming characteristics (corresponding to the eigenvalues λ_2 and λ_3) are given values from the interior points closest to the boundary points. This boundary treatment works well for sound waves (demonstrated for circular sound waves in [24]), but it gives some reflections for large amplitude gravity waves. However, this is not a problem in the physical situation we consider here, because downwards propagating gravity waves are exponentially damped by the stratification of the atmosphere, and the critical level formed by the shear flow acts as a barrier for the upward propagation of gravity waves. As a result, only small amplitude gravity waves reach the upper and lower boundaries, and they are handled satisfactorily by these boundary conditions.

4. THE SPECTRAL VISCOSITY METHOD

We will briefly describe the spectral viscosity method in this section. For non-linear conservation laws, the solution of the standard spectral method does not converge to the correct entropy solution if the solution contains shocks. Some small artificial viscosity can be added to the model such that the solution will converge to the exact and physically relevant solution as the viscosity tends to zero. If the viscosity coefficient decreases as the number of grid points increases, a finite degree of accuracy can be obtained. Tadmor [22] introduced the spectrally vanishing viscosity, which in addition acts only on frequencies higher than a certain threshold frequency, and it was shown that the method did converge to the unique entropy solution for the inviscid Burgers' equation, assuming that the solution was uniformly bounded. Spectral accuracy was obtained by letting the threshold frequency increase with the number of points. Further studies of the convergence of the method includes [15, 16, 19, 21], and the conditions are given in [23] as follows:

Consider the 2π-periodic system of conservation laws

$$\frac{\partial u(x,t)}{\partial t} + \frac{\partial f(u)}{\partial x} = 0, \qquad u(x,0) = u_0(x), \tag{8}$$

together with a given entropy condition, and apply the SV method on the form

$$\frac{\partial u^N}{\partial t} + \frac{\partial}{\partial x}[P_N f(u^N)] = \varepsilon_N \frac{\partial}{\partial x}\left(Q * \frac{\partial u^N}{\partial x}\right), \qquad u^N(x,0) = u_0(x), \tag{9}$$

where $u^N = u^N(x,t) = \sum_{k=-N}^{N} a_k(t)\, e^{ikx}$ is the numerical solution and P_N is a projection operator upon the space of trigonometric polynomials of degree N. The right-hand side of (9) involves the convolution of the spectral viscosity kernel

$$Q = Q(x,t) = \sum_{m_N \leq |k| \leq N} k^2 \hat{Q}_k(t)\, e^{ikx} \tag{10}$$

and the first derivative of u^N. In spectral space, this right-hand side is calculated as

$$-\varepsilon_N \sum_{m_N \leqslant |k| \leqslant N} k^2 \hat{Q}_k(t)\, a_k(t)\, e^{ikx}. \tag{11}$$

The parameters in the SV method are the viscosity amplitude ε_N, the coefficients $\hat{Q}_k(t)$, and the frequency m_N, where the viscosity starts to act. The dissipation introduced through the spectral viscosity term must be large enough to ensure that u^N converges to the entropy solution of (8) as $N \to \infty$ and small enough to retain spectral accuracy. If u^N is uniformly bounded ($\|u^N\|_{L^\infty(x,t)} \leqslant C$), then convergence is obtained if

$$\varepsilon_N \geqslant 1/N, \qquad \hat{Q}_k \geqslant \text{Const} - \frac{1}{\varepsilon_N k^2}. \tag{12}$$

The spectral viscosity term (11) is kept spectrally small and spectral accuracy is retained, if

$$\varepsilon_N \sim \frac{1}{N} \quad \text{and} \quad m_N \sim N^\beta, \qquad \beta < \frac{1}{2}. \tag{13}$$

The SV method with Chebyshev polynomials has not yet been fully analysed, but the following implementation of the viscosity term has been suggested by Tadmor (private communication) [20]:

$$\frac{\varepsilon_N}{w(x)^p} \frac{\partial}{\partial x}\left(R * \frac{u_x^N}{w(x)^q}\right)$$

$$\text{with} \quad R * \frac{u_x^N}{w(x)^q} = \sum_{m_N < l < N} \hat{R}_l \tilde{b}_l(t)\, T_l. \tag{14}$$

In (14), $w(x) = (1-x^2)^{-1/2}$ is the Chebyshev weight function, the exponents p and q are parameters to be chosen later, and $\sum_{l=0}^{N} \tilde{b}_l(t)\, T_l$ is the Chebyshev representation of the weighted first derivative $1/w(x)^p\, u_x^N$. The parameters can be chosen as [20]

$$\varepsilon_N \sim \frac{1}{N}, \qquad m_N \sim N^{1/2},$$
$$\hat{R}_k \geqslant 1 - \left(\frac{m_N}{k}\right)^2 \qquad \text{for} \quad k > m_N. \tag{15}$$

To apply the SV method to the problem (1), spectral viscosity terms must be added to Eqs. (5). These terms are denoted by tildes and subscripts xx or zz, where

$$\tilde{u}_{xx}^V = \frac{\partial}{\partial x}\left(Q * \frac{\partial u^V}{\partial x}\right),$$
$$\tilde{u}_{zz}^V = \frac{1}{w(z)^p} \frac{\partial}{\partial z}\left(R * \frac{u_z^V}{w(z)^q}\right). \tag{16}$$

Different kinds of spectral viscosity terms can be added to the inviscid model (5), and a straightforward choice is to add the following vector at the right-hand side:

$$(\varepsilon_M \tilde{\rho}_{xx}^V + \varepsilon_N \tilde{\rho}_{zz}^V, \varepsilon_M \tilde{u}_{xx}^V + \varepsilon_N \tilde{u}_{zz}^V, \varepsilon_M \tilde{v}_{xx}^V$$
$$+ \varepsilon_N \tilde{v}_{zz}^V, \varepsilon_M \tilde{\rho}_{xx}^V + \varepsilon_N \tilde{\rho}_{zz}^V)^T. \tag{17}$$

Another possibility is to mimic the physical diffusion terms and use

$$(0, \varepsilon_M \tilde{u}_{xx}^V + \varepsilon_N \tilde{u}_{zz}^V, \varepsilon_M \tilde{v}_{xx}^V + \varepsilon_N \tilde{v}_{zz}^V, \kappa_M \tilde{T}_{xx}^V + \kappa_N \tilde{T}_{zz}^V)^T, \tag{18}$$

where $T^V = p^V/\rho^V$ is the normalized temperature, and κ_M, κ_N are "spectral thermal diffusion" amplitudes. Regardless of the physical origins of the diffusion terms, like viscosity or heat diffusion, they will be called spectral viscosity terms in the following. The use of (17) and (18) are compared in the numerical experiments in Section 6.

5. THE ODE-SOLUTION

In this section we will describe the application of ODE-solvers to the ODE-system resulting from a spectral discretization in space and discuss accuracy and stability properties with and without spectral viscosity.

As a model problem consider the linear hyperbolic system

$$u_t + Au_x = b, \qquad A \in \mathbb{R}^{k \times k}, \tag{19}$$

and its discretization by spectral collocation with N points:

$$u_t^N + (A \otimes D)\, u^N = B, \qquad u^N \in \mathbb{R}^{Nk}, \tag{20}$$

where D is the derivative matrix, see, e.g., [4]. The operator $\otimes$ is the Kronecker product, see, e.g., [12, Chap. 12].

The Jacobian of this ODE-system is $J = -A \otimes D$ and it is well known that J is full and that the spectral radius is $\rho(J) = O(N^2)$ in the Chebyshev case and $O(N)$ in the Fourier case, thus indicating stiffness for large N. In two space dimensions the Jacobian is of the form:

$$A_1 \otimes I_y \otimes D_x + A_2 \otimes D_y \otimes I_x,$$

where A_1, A_2 are coefficient matrices, D_x and D_y are derivative matrices in the x- and y-direction, respectively, and I_x, I_y are identity matrices. We see that the spectral radius of this Jacobian is not larger than the sum of the spectral radii for the one-dimensional problems. The choice between explicit or implicit methods is not trivial for spectral discretizations. Using a conventional implicit ODE-solver with modified Newton iteration to solve the non-linear equations is very time-consuming, because the

Jacobian and hence the Newton matrix is full. For large N the method is not useful in practice since most ODE-solvers use direct methods to solve the linear equations in the Newton iteration. In [14] we have shown how to use an implicit solver with an iterative solver for the linear systems. This seems to work well, provided one can find appropriate preconditioners. For some test problems the time-steps using an implicit solver were much larger than for an explicit method, see [14], so if the ODE-system is stiff in a large part of the integration interval such implicit methods can be an interesting alternative. If the solution varies rapidly throughout the integration interval, explicit methods will usually be more efficient since they are much cheaper computationally and the time-step is often constrained by accuracy rather than stability.

One additional point to this discussion is the boundary treatment. As explained above, a boundary correction technique is used, correcting the boundary values after performing a time-step. Such a procedure is not meaningful for implicit methods. This point is addressed in [5] and further analysed in [2], where the resulting ODE-system including the boundary conditions is given in a closed form for general quasi-linear hyperbolic systems.

In the following we will discuss the use of explicit solvers only. There exist quite a few good codes based on explicit methods; some of them are mentioned in [10]. We use the following terminology: For a generic ODE-system

$$U_t = f(t, U);$$

the term function evaluation means the evaluation of the right-hand side of the ODE-system. Important issues in choosing ODE-solvers are the accuracy requirements and the cost of a function evaluation. In our case the acuracy requirements are moderate in the ODE sense (error tolerances set to 10^{-4}–10^{-6}, say) and the cost of a function evaluation is high, hence pointing to a low order method. We have to use a one-step method because of the boundary correction procedure. The widely used Runge–Kutta codes RKF45 and DOPRI5(4) (see [10]) uses 6- and 7-function evaluations per step, respectively, which we regard as too costly. We have chosen to use the second-order improved Euler scheme, here called RK2, with the following Butcher tableau:

$$\begin{array}{c|cc} 0 & 0 & \\ 1/2 & 1/2 & \\ \hline b & 0 & 1 \end{array} \tag{21}$$

We want to use variable time-steps, and since the first stage of the method is a forward Euler step we may use embedding and local extrapolation (see [10, Section II.4]) denoted by RK2(1). However, for our purposes we prefer to use the RK2(3) scheme, with Butcher tableau shown below, because the time-steps chosen were larger than for RK2(1), giving a smaller total cost in terms of CPU time:

$$\begin{array}{c|ccc} 0 & 0 & & \\ 1 & 1 & & \\ 1/2 & 1/4 & 1/4 & \\ \hline b & 1/2 & 1/2 & \\ \hline \hat{b} & 1/6 & 1/6 & 4/6 \end{array} \tag{22}$$

If y_{n+1} is the result of the improved Euler step and $\tilde{y}_{n+1}$ is the result of the error estimation, the logic for determination of the time-step is based on the size of the error indicator $\|e_{n+1}\| = \|y_{n+1} - \tilde{y}_{n+1}\|$ with an appropriate norm (for examples of this technique, see [10, Appendix]).

The stability plot of the basic scheme is shown in Fig. 1. As mentioned above, $\rho(J) = O(N^2)$ and with the stability region as shown, the typical and well-known stability restriction on the time-step is $O(N^{-2})$.

In order to study the accuracy characteristics for the RK2(3) scheme in more detail, we compute the error term for the model problem. Let $M = A \otimes D$, denote by U_n the vector of unknowns at time t_n, and let h be the current time-step: $h = t_{n+1} - t_n$. The stage values are

$$Y_1 = U_n,$$

$$Y_2 = U_n - \frac{h}{2} MU_n + B,$$

$$Y_3 = U_n + \frac{h}{4}\left(-2MU_n + 2B + \frac{h}{2} M^2 U_n - \frac{h}{2} MB \right).$$

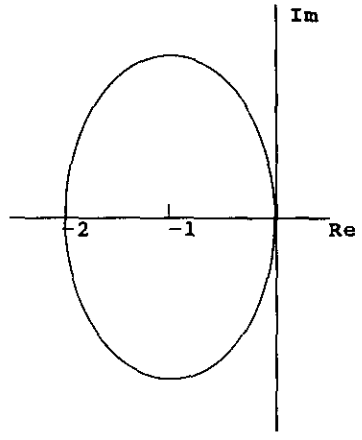

FIG. 1. Stability plot for RK2.

The error term is now

$$e_{n+1} = \frac{h}{3}(k_1 + k_2 - 2k_3) = \frac{h^3}{12} M^2(-MU_n + B), \quad (23)$$

where $k_i = f(t, Y_i)$ (cf. the generic ODE-system).

Looking at a single equation

$$U_t + aU = B, \qquad a \in \mathbf{C}, \quad (24)$$

the time-step is chosen such that

$$\frac{h^3}{12} |-|a|^3 U_n + |a|^2 B| \approx \text{atol} + \text{rtol}\,|U_n|. \quad (25)$$

where *atol* and *rtol* are the absolute and relative error tolerances, respectively. Letting $B \equiv 0$, we see that

$$\text{atol} \ll \text{rtol}\,|U_n| \Rightarrow h_1 \approx \frac{(12\,\text{rtol})^{1/3}}{|a|}, \quad (26)$$

$$\text{atol} \gg \text{rtol}\,|U_n| \Rightarrow h_2 \approx \left(\frac{12\,\text{atol}}{|U_n|}\right)^{1/3} \frac{1}{|a|}. \quad (27)$$

We want to choose the error tolerances such that the time-step will be the largest possible. Note that for an ODE-system we may choose the error tolerances individually for each component, so it is appropriate to discuss the scalar case. We see that pure relative error control is not efficient for $|U_n|$ small, since $|U_n|$ does not enter in the expression (26). The time-step h_2 is larger than h_1 for $|U_n|$ small and atol $\approx$ rtol; hence mixed error or absolute error control is to be preferred. In the case $B \neq 0$ we will reach almost the same conclusion: The mixed error control is the most efficient.

If the Jacobian is diagonalizable, the ODE-system in (20) can be transformed into a set of scalar ODEs of the form (24) where a represents the eigenvalues of the Jacobian. From (26) and (27) we then see that the time-step is determined by the equation with the largest $|a|$ in this set with non-negligible solution component. For example, if components with large $|a|$ ("high frequency") have small amplitudes in the first phase of the integration, but will obtain larger amplitudes in a later phase, the time-step will drop, provided that the time-step is accuracy-bounded. This explains the drop in time-step in a non-linear system in a phase where "energy" is transferred from low to high frequencies. On the other hand, the time-step restriction by stability is independent of the amplitude of the solution components; this constraint is in action throughout the integration interval.

To sum up, the time-step behaviour is determined by the stability restrictions as well as the "frequency" and amplitude of each solution component.

Consider now the behaviour of the different solution components during a typical simulation run, using an explicit method for time integration. The acoustic waves (which are of no interest in the present context) will determine a stability restriction throughout the integration interval. The time-steps are accuracy-bounded by the acoustic waves in the transient region, i.e., until these waves have left the simulation domain. The amplitudes of the gravity wave components are fairly small before the more turbulent state is reached and these components will not restrict the time-step in this region. With an implicit ODE-solver we may expect to obtain larger time-steps in the (comparatively long) interval where the time-step is mainly stability-restricted. When the turbulent state is reached, components with high spatial frequencies increase in amplitude and, if no damping mechanism is introduced, the time-step will be dropping because of the accuracy requirements of these components.

Before we discuss the time integration aspects of the SV method, let us briefly present the quasi-linear model problem:

$$u_t + A(u)\,u_x = b, \qquad u \in \mathbb{R}^k. \quad (28)$$

If we discretize in space by spectral collocation, we obtain

$$u_t^N + \{\text{diag}(a_{ij}(u^N))\}_{i,j=1}^k \cdot (I_k \otimes D)\,u^N = B. \quad (29)$$

Note that $a_{ij}(u^N)$ have values in $\mathbb{R}^N$ such that the matrix $\text{diag}(a_{ij}(u^N))$ is a $kN \times kN$ diagonal matrix. The Jacobian is now

$$J = -\{\text{diag}(a_{ij}(u^N))\}_{i,j=1}^k \cdot (I_k \otimes D) - \left\{\text{diag}\left(\sum_{m=1}^k Du_m^N \odot \frac{\partial a_{im}(u^N)}{\partial u_j^N}\right)\right\}_{i,j=1}^k, \quad (30)$$

where $u^N = [u_1^N, \ldots, u_k^N]$, $u_i^N \in \mathbb{R}^N$, and $\odot$ denotes the componentwise product of two vectors in $\mathbb{R}^N$. The non-linearity enters in the second term, and in general it is difficult to determine whether its contribution is significant. Two important issues in this context are how fast the solution components vary and the form of the derivatives in the term.

Spectral viscosity is a means to reduce the buildup of solution components with high spatial frequency, and we can therefore expect a less dramatic time-step reduction when the unperturbed problem contains solution components with high frequency.

We consider the SV method of the form (14) applied to the model problem,

$$u_t^N + A(u^N)\frac{\partial u^N}{\partial x} = \frac{\varepsilon_N}{w(x)^p}\frac{\partial}{\partial x}\left(R * \frac{u_x^N}{w(x)^q}\right) + B, \quad (31)$$

where

$$R * \frac{u_x^N}{w(x)^q} = \sum_{m_N < k < N} \hat{R}_k \tilde{b}_k T_k, \tag{32}$$

$w(x)$ is the Chebyshev weight function, and $\sum_{k=0}^{N} \tilde{b}_k T_k$ is the Chebyshev representation of the weighted first derivative $1/w(x)^q\, u_x^N$.

We will now express the spectral viscosity term in matrix form in order to find the Jacobian matrix for the discretized system. Let $u_x^N = \{\{u_{1,x}^N(x_j)\}_{j=0}^N, \ldots, \{u_{k,x}^N(x_j)\}_{j=0}^N\}$. Then we have $u_x^N = (I_k \otimes \mathscr{F}^{-1})\tilde{b}$, where $\tilde{b}$ is the vector of Chebyshev coefficients and $\mathscr{F}$ is the (nonsingular) transformation matrix. Hence we obtain $\tilde{b} = (I_k \otimes \mathscr{F})\, u_x^N$. The spectral derivative is computed as $u_x^N = (I_k \otimes D)\, u^N$ and the viscosity second derivative corresponding to the convolution above is denoted by $\tilde{u}_{xx}^N = (I_k \otimes D) \cdot (I_k \otimes \tilde{D})\, u^N$.

From the definition we have: $\tilde{u}_{xx}^N = (I_k \otimes D) \cdot (I_k \otimes \mathscr{F}^{-1}) \cdot (\tilde{b} \odot R)$, where $\odot$ denotes the componentwise product. Then

$$\begin{aligned} \tilde{u}_{xx}^N &= (I_k \otimes D) \cdot (I_k \otimes \mathscr{F}^{-1})((I_k \otimes \mathscr{F}) \cdot (I_k \otimes D)\, u^N \odot R) \\ &= (I_k \otimes D) \cdot (I_k \otimes \mathscr{F}^{-1}) \cdot \operatorname{diag}(R) \cdot (I_k \otimes \mathscr{F} D)\, u^N \\ &= (I_k \otimes D) \cdot \mathscr{E} \cdot (I_k \otimes D)\, u^N, \end{aligned} \tag{33}$$

where $\mathscr{E} = (I_k \otimes \mathscr{F}^{-1}) \cdot \operatorname{diag}(R) \cdot (I_k \otimes \mathscr{F})$.

For the quasi-linear model problem we then obtain the spectral discretization

$$\begin{aligned} u_t^N + \{\operatorname{diag}(a_{ij}(u^N))\}(I_k \otimes D)\, u^N \\ = (I_k \otimes D) \cdot \mathscr{E} \cdot (I_k \otimes D)\, u^N + B. \end{aligned} \tag{34}$$

The contribution to the Jacobian from the spectral viscosity term is (for both linear and quasi-linear problems): $(I_k \otimes D) \cdot \mathscr{E} \cdot (I_k \otimes D)$. The question is now what spectral properties this modified Jacobian has, because that determines the stability restrictions for the ODE-solution. It seems difficult to try to determine the spectrum of the modified Jacobian directly, so we will investigate it numerically as a part of the experiments reported in Section 6.

We may also compute the error term for the quasi-linear model problem, but it is not given here because it is fairly complicated and no further insight seems to be gained from that complicated expression. The derivation is entirely similar to the linear case.

If we write the Jacobian with spectral viscosity as

$$J(\varepsilon_N) = J_0 + \varepsilon_N (I_k \otimes D) \cdot \mathscr{E} \cdot (I_k \otimes D), \tag{35}$$

where J_0 is the Jacobian given in (30) and $\varepsilon_N \in \mathbb{R}$, we can regard the spectral viscosity term as a perturbation to the original matrix: $J(\varepsilon_N) = J_0 + \varepsilon_N J_1$. We can therefore use a theorem due to Motzkin, see [11, p. 96], saying that if $J(\varepsilon_N)$ is diagonalizable for all ε_N then

$$\lambda(J(\varepsilon_N)) = \lambda(J_0) + \varepsilon_N \lambda(J_1). \tag{36}$$

Hence the problem reduces to find $\lambda(J_1)$ (which is far from trivial) since it is assumed that we know $\lambda(J_0)$. In the cases where ε_N is small (say $1/N$ or smaller) the contribution to the spectrum from the perturbation will be modest. As the parameters in (15) suggest and from what the numerical experiments below show, ε_N have to be fairly small in order not to perturb the solution. Hence we can expect that the SV method will not alter the stability restriction significantly; its main effect will be to prevent energy from being built up on higher frequencies.

6. NUMERICAL RESULTS

The numerical method described in the previous sections is applied to the problem of gravity wave/wind shear interaction outlined in Section 2. The two computational domains are illustrated in Fig. 2. Gravity waves are generated in the forcing layer in the lower domain, and the wind profile is chosen such that the critical level is formed in the middle of the upper domain. All results presented will be from the upper domain, where the most interesting features of the solution are found.

We first present calculations with the inviscid model (5). The evolution of potential temperature with 128×129 collocation points in each of the two domains is shown in Fig. 3. Initially, the level curves are equidistant horizontal straight lines, but at $t = 40$ they are almost vertical in a part of the domain, indicating adiabatic equilibrium ($d\theta/dz = 0$). As the simulation proceeds, the waves "break" and local convective instabilities occur, leading to a more complex pattern. Figure 4 shows the time-steps chosen by the adaptive ODE-solver for calculations with different numbers of

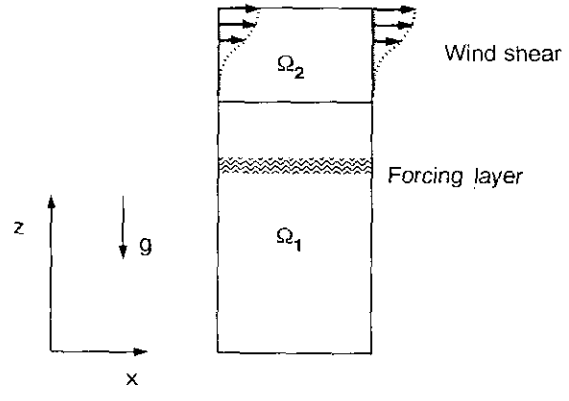

FIG. 2. The two computational domains of the numerical calculations, with forcing layer and area of wind shear.

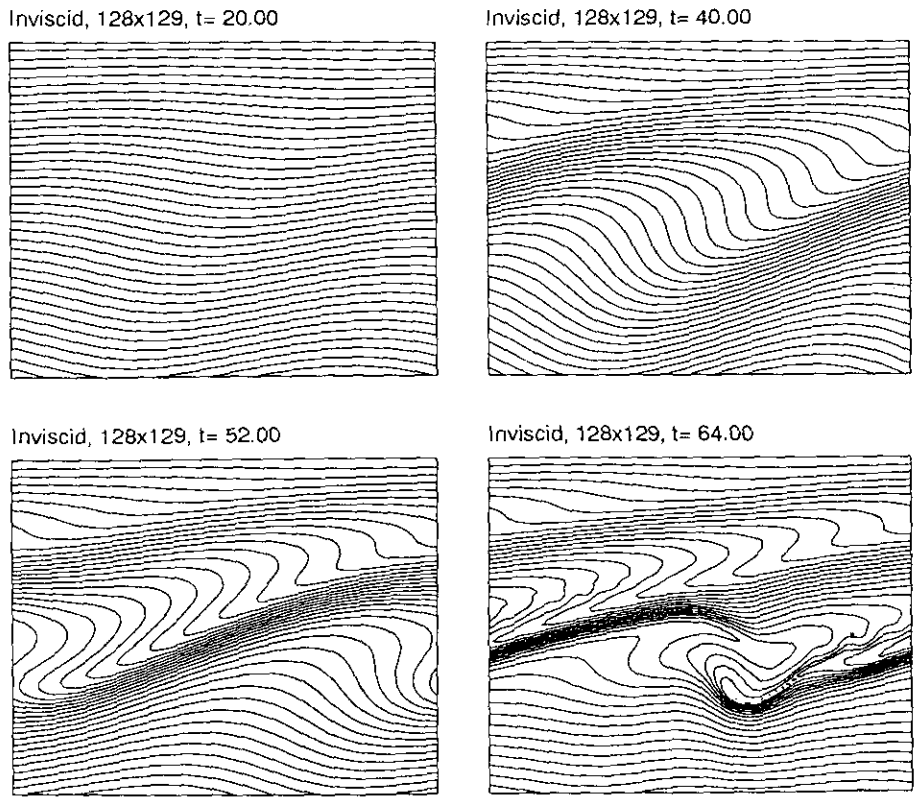

FIG. 3. Level curves for the logarithm of potential temperature, inviscid model.

points. In the first phase of the calculations, the time-steps are chosen according to stability considerations, and we obtain $\Delta t \sim 6/N^2$, where N is the number of points in the vertical (Chebyshev) direction. But as the instabilities start to dominate, the time-steps are restricted by accuracy requirements, and drop quickly. The stability-restricted period is longer for finer grids, but when the time-steps start to drop they drop faster for the finer grids, because higher frequencies become more dominating than for the coarse grids, cf. the time-step restrictions given by (26) and (27). An inviscid "reference" solution would be desirable for comparisons with the spectral viscosity results presented below, but even with 128×129 points the inviscid simulation broke down after just above 66 time units.

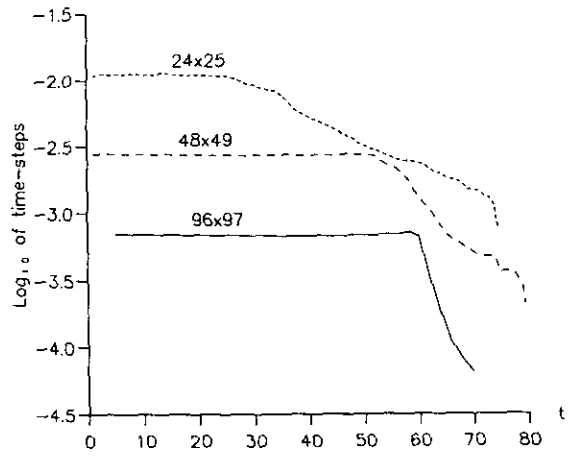

FIG. 4. Time-steps for different numbers of points, inviscid model.

To illustrate the problem of energy transfer, Fig. 5 shows the logarithm of the amplitude of the spectral coefficients $\{a_{n/2,n}\}_{n=0}^{N}$ from (4) for the physical variables after 58 time units. Coefficients from a simulation with 24×25 points are represented by crosses, and the corresponding part of the spectrum from the 128×129-calculation is shown by circles. The lower coefficients are similar in the two simulations, but the higher coefficients from the 24×25-simulation are larger because the energy cannot be transferred to higher frequencies.

We now turn to the application of the SV method. Unless otherwise noted, the spectral viscosity terms (18) are added to the right-hand side of inviscid equations (5). To evaluate different forms of the spectral viscosity terms and the choice of parameters, we shall examine the numerical solution, its spectral coefficients, and the time-steps chosen by the adaptive ODE-solver. The numerical solution should neither contain non-physical oscillations nor excessive damping, and it should be in accordance with solutions with higher

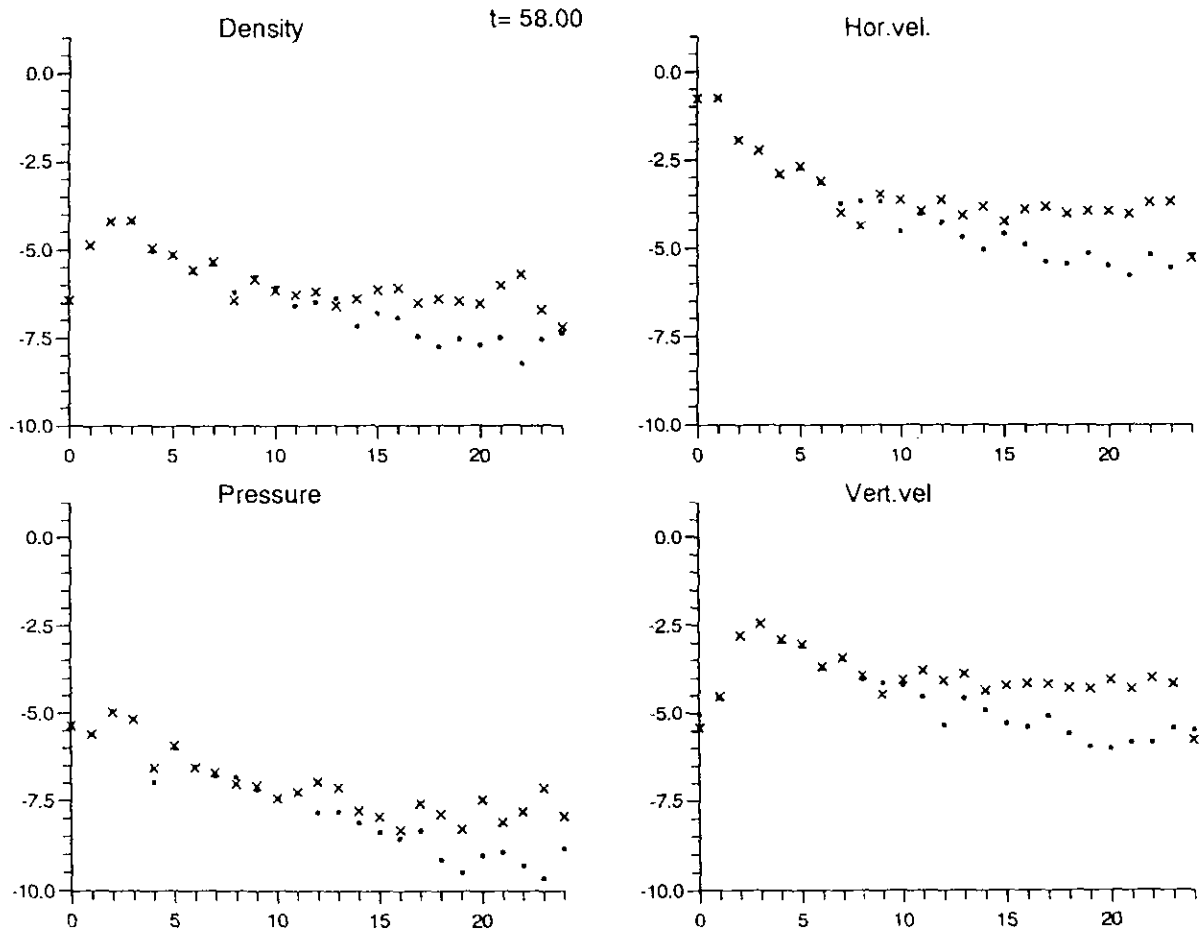

FIG. 5. The logarithm of the coefficients $\{a_{n/2,n}\}_{n=0}^{N}$ for $N=24$ (crosses) and $N=128$ (circles) at $t=58$, inviscid model.

resolution and with the inviscid "reference" solution as far as this could be calculated. The spectral coefficients for low frequencies, carrying most of the energy, should be influenced as little as possible by the spectral viscosity terms, but the amplitudes should decay at the high end of the spectrum to indicate that energy is not artificially piled up at the highest frequencies. The time-steps should be restricted only by stability considerations in the first part of the simulations, and then drop according to the accuracy requirements, but level out at an acceptably low level when the spectral viscosity terms balance the non-linear energy cascade. To be able to do lots of experiments at a reasonable cost, the spectral viscosity tests were mainly run with 24×25 or 32×33 points in each domain.

Experiments were carried out with different values of the exponents p and q in the Chebyshev spectral viscosity terms from (16); $p>0$ means that the equations become hyperbolic at the upper and lower boundaries, which means that the boundary and interface conditions from the inviscid case can be left unchanged. Time-steps from two typical simulations (32×33 points) with $q=0$ and $q=1$, respectively ($p=1$ in both cases), are shown in Fig. 6. We observe that the time-steps are slightly smaller during most of the simulation for $q=1$, which indicates that $q=0$ gives a more well-behaved ODE-system. In particular, the time-steps for $q=1$ are not in equilibrium at the stability limit in the first part of the simulation, when the spectral viscosity terms should

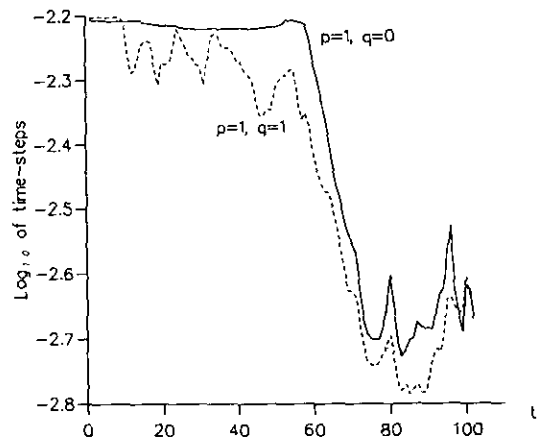

FIG. 6. Time-steps for typical simulations with different values of the Chebyshev weight function exponents.

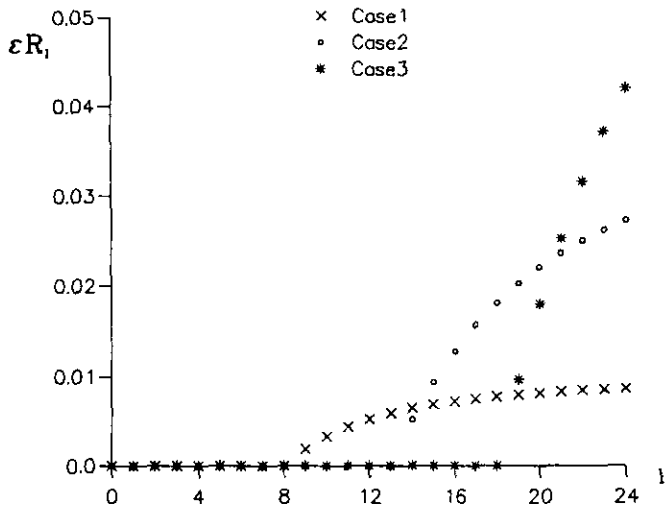

FIG. 7. Three different filters.

be of small importance. The numerical solutions from these simulations are almost indistinguishable, but we can observe some small wiggles near the upper and lower boundaries for $q = 1$, which is explained by the fact that the weight functions reduce the effect of the spectral viscosity in these areas. The calculations presented below are run with $p = 1$, $q = 0$.

The viscosity amplitudes, threshold frequencies, and viscosity coefficients for the x-direction are chosen according to (12), (13) as

$$\varepsilon_M = \varepsilon/M, \qquad \kappa_M = \kappa/M, \qquad m_M = C_x M^{1/2},$$
$$\hat{Q}_k = \begin{cases} 0, & 0 \leqslant |k| \leqslant m_M, \\ 1 - (m_M/k)^2, & m_M < |k| \leqslant M/2, \end{cases} \tag{37a}$$

and for the z-direction, according to (15), as

$$\varepsilon_N = \varepsilon/N, \qquad \kappa_N = \kappa/N, \qquad m_N = C_z N^{1/2},$$
$$\hat{R}_l = \begin{cases} 0, & 0 \leqslant l \leqslant m_N, \\ 1 - (m_N/l)^2, & m_N < l \leqslant N. \end{cases} \tag{37b}$$

This leaves us with the parameters ε, κ, C_x, and C_z to vary.

The argument in Section 2 concerning the "numerical" Prandtl number indicated that $\varepsilon/\kappa = 100$ should be a good

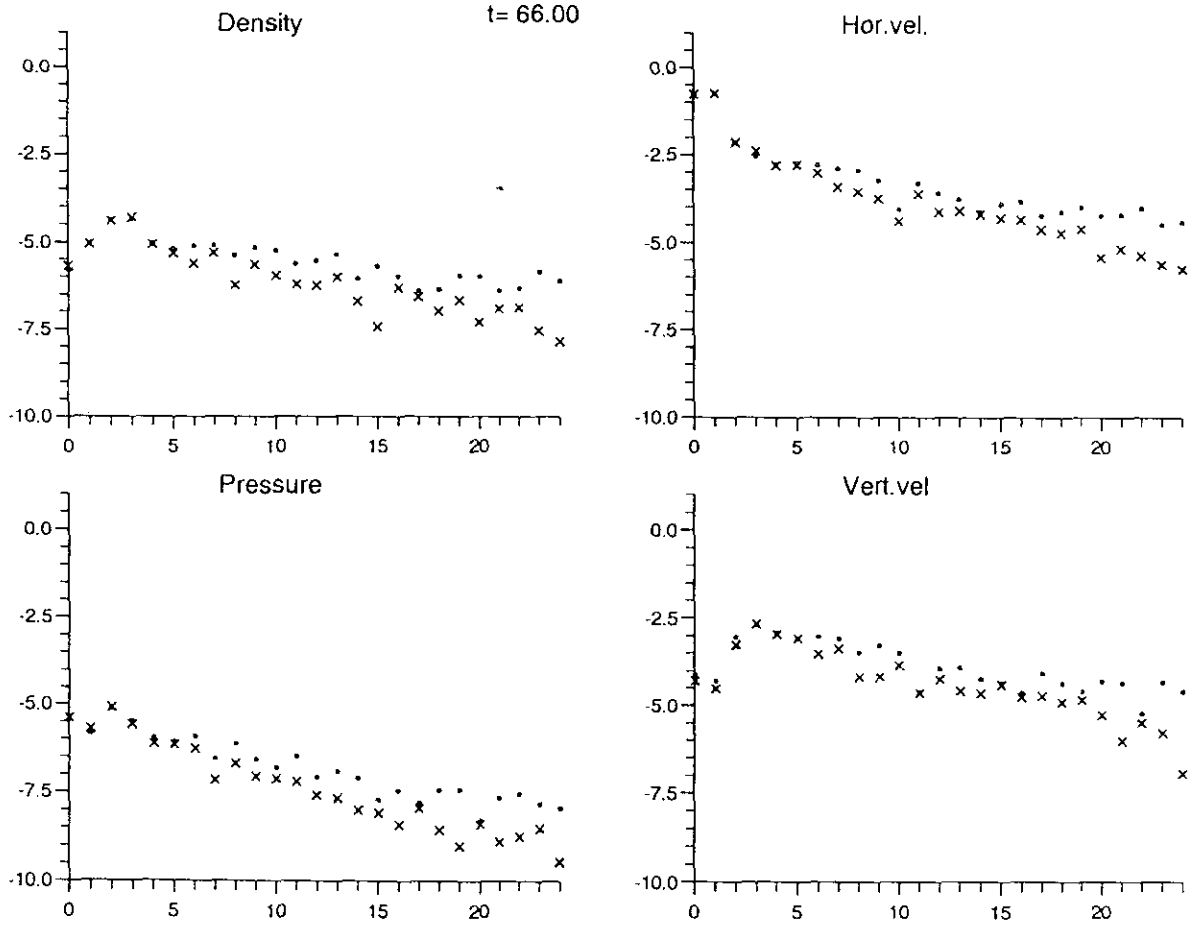

FIG. 8. The logarithm of the coefficients $\{a_{n/2,n}\}_{n=0}^{N}$ from runs with 24×25 points and the spectral viscosity parameters (38a) (Case 1) are shown with crosses. Corresponding coefficients from an inviscid simulation with 128×129 points are shown with circles.

choice, and this is confirmed by numerical experiments. Keeping this ratio, we shall present results for three different combinations of parameters:

$$\text{Case 1,}\quad C_x = 1.0,\quad C_z = 2.0,\quad \varepsilon = 0.01,\quad \kappa = 0.0010, \tag{38a}$$

$$\text{Case 2,}\quad C_x = 1.5,\quad C_z = 3.0,\quad \varepsilon = 0.04,\quad \kappa = 0.0004, \tag{38b}$$

$$\text{Case 3,}\quad C_x = 2.0,\quad C_z = 4.0,\quad \varepsilon = 0.10,\quad \kappa = 0.0001. \tag{38c}$$

The Chebyshev filter coefficients $\hat{R}_l$ multiplied by ε for these three cases are shown in Fig. 7 for $N = 24$. The right balance between viscosity amplitude and threshold frequency must be found. Figures 8–10 show the amplitude of the spectral coefficients $\{a_{n/2,n}\}_{n=0}^{N}$ from (4) for the four physical variables at $t = 66$, with 24×25 points and the three sets of parameters given above. The corresponding coefficients from the 128×129 points simulation without spectral viscosity are plotted as circles for comparison.

For Case 1 (Fig. 8), it looks as though the viscosity amplitudes could have been reduced, because most of the coefficients are smaller than for the inviscid run, but reduced amplitudes resulted in smaller time-steps and no improvement of the solution. For Case 3 (Fig. 10), we see the damping effect on the highest coefficients, but the middle part of the spectrum contains more energy than the corresponding part of the inviscid spectrum, as if a reflection of energy in spectral space has taken place. This indicates that a strong damping at the high end of the spectrum only is not favourable. Case 2 (Fig. 9) represents a middle way between Case 1 and Case 3, and here the lower $\frac{2}{3}$ of the coefficients are close to the inviscid values, while the upper third decay faster.

Time-step information for the three cases are shown in Fig. 11, and we obtain another indication of insufficient damping in Case 3 from the shorter time-steps towards the end of the simulation. An inviscid run with 24×25 points is also included, and the typical difference in time-step

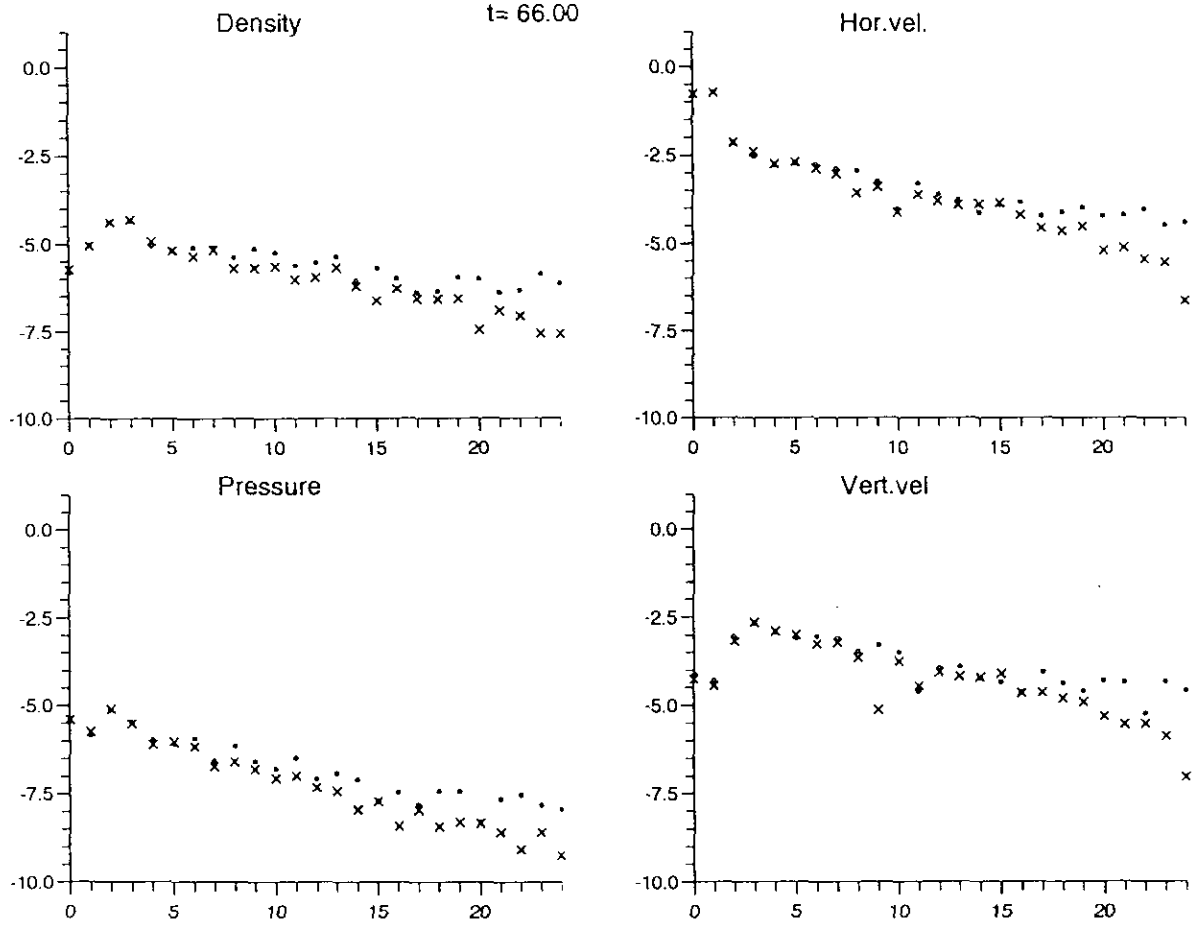

FIG. 9. The logarithm of the coefficients $\{a_{n/2,n}\}_{n=0}^{N}$ from runs with 24×25 points and the spectral viscosity parameters (38b) (Case 2) are shown with crosses. Corresponding coefficients from an inviscid simulation with 128×129 points are shown with circles.

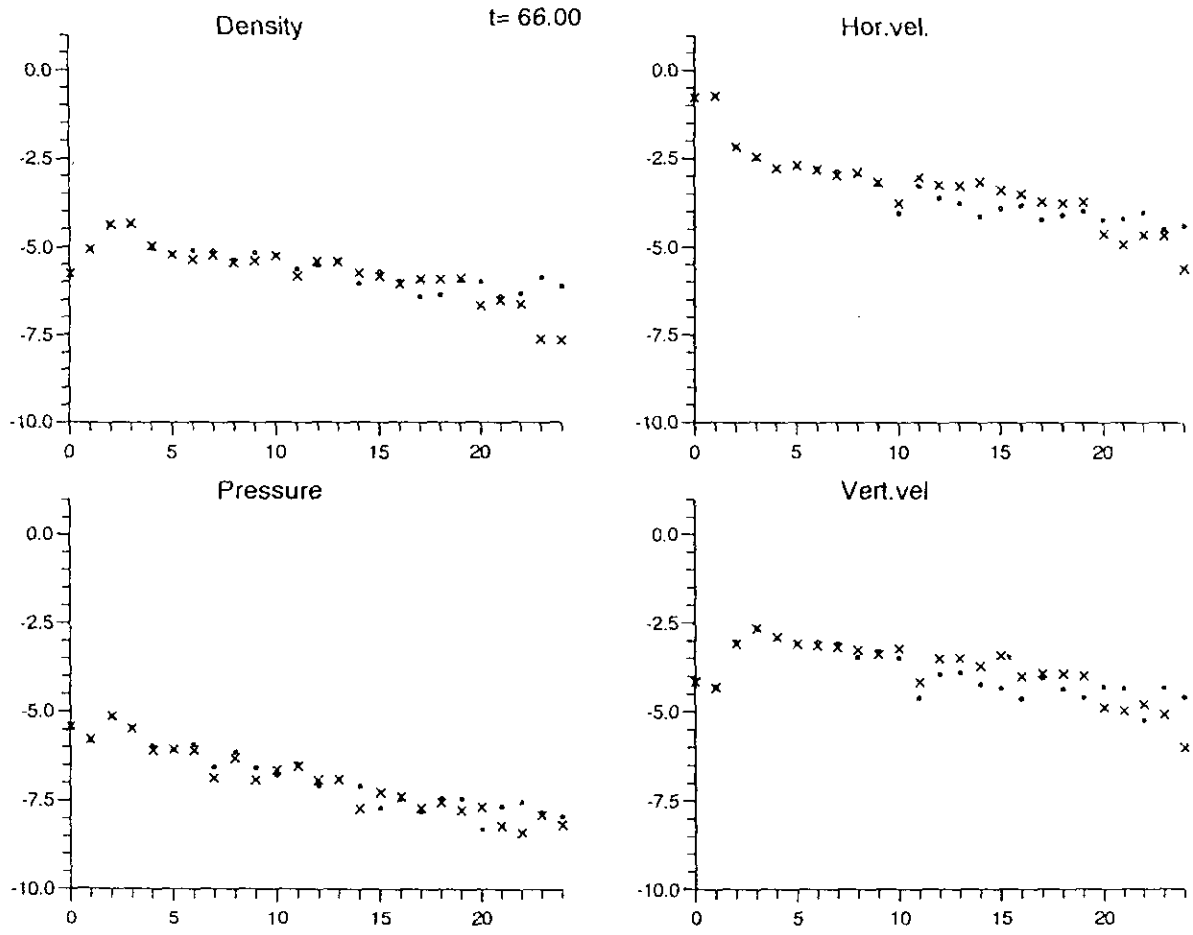

FIG. 10. The logarithm of the coefficients $\{a_{n/2,n}\}_{n=0}^{N}$ from runs with 24×25 points and the spectral viscosity parameters (38c) (Case 3) are shown with crosses. Corresponding coefficients from an inviscid simulation with 128×129 points are shown with circles.

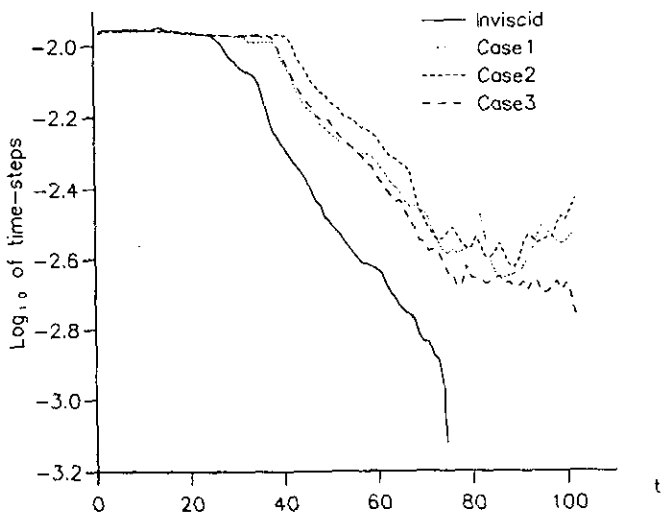

FIG. 11. Time-steps from runs with the three sets of spectral viscosity parameters (38a)–(38c) and an inviscid run, 24×25 points.

behaviour is clearly demonstrated. The time-steps from the SV simulations stay for a longer time at the stability limit, and they level out in less structured behavior at a later stage when the inviscid simulation breaks down. The SV method as implemented here involves 50% more transforms between physical and spectral space than the inviscid method in order to calculate the filtered second derivatives. As the transforms are the main time-consuming elements in the code, the SV method requires about 1.5 times the computer time of the inviscid method per time-step. However, from Fig. 11 we see that the time-steps from the SV method are roughly a factor two larger than for the inviscid method when they are dropping, and this phase involves many more time-steps than the first phase with stable time-steps. A closer study of the time-steps shows that for these simulations, the SV method (Case 2) with the same number of points is more effective than the inviscid method for integration of more than around 60 time units, i.e., even before the latter really breaks down. We also mention that the extra

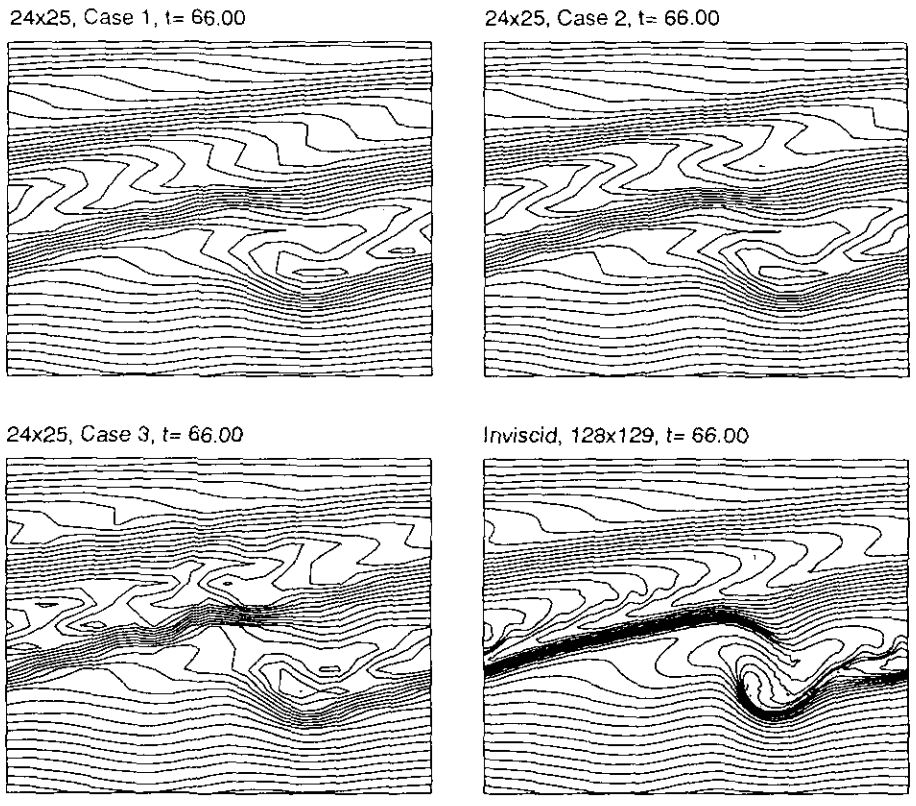

FIG. 12. Level curves for the logarithm of the potential temperature at $t = 66$ from runs with the three sets of spectral viscosity parameters (38a)–(38c) with 24×25 points and an inviscid "reference" run with 128×129 points.

transforms required can be done in parallel with the original transforms.

The potential temperature at $t = 66$ with the same three sets of parameters are plotted in Fig. 12, together with the inviscid 128×129 "reference" solution which required about 200 times as much computer time. Of course the results obtained with only 24×25 points are quite rough, but the important thing is to check which of the SV runs that has captured most of the main features correctly. We observe that much of the overturning of the wave is lost in Case 1 as a result of too much smoothing, while Case 3 clearly suffers from too little smoothing. The figure also shows the numerical oscillations that occur at this final stage of the inviscid calculation.

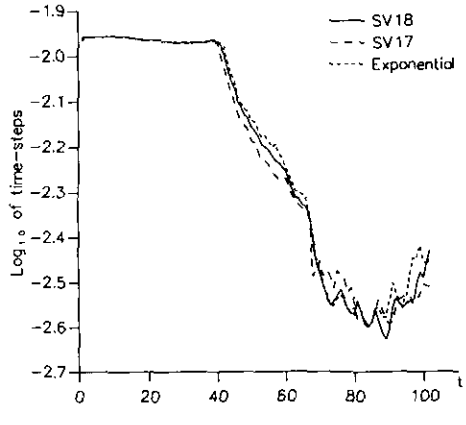

FIG. 13. Time-steps for runs with different spectral viscosity implementations.

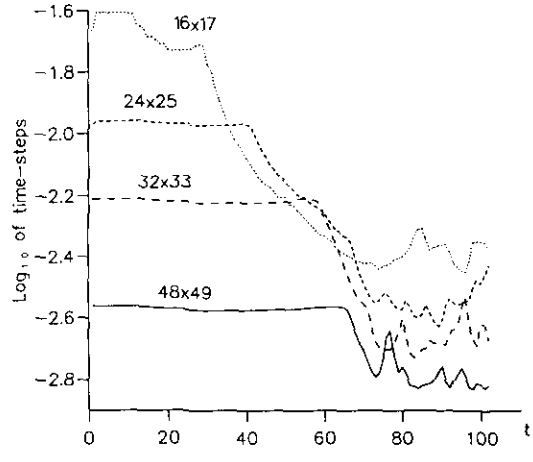

FIG. 14. Time-steps for runs with same parameters, different numbers of points.

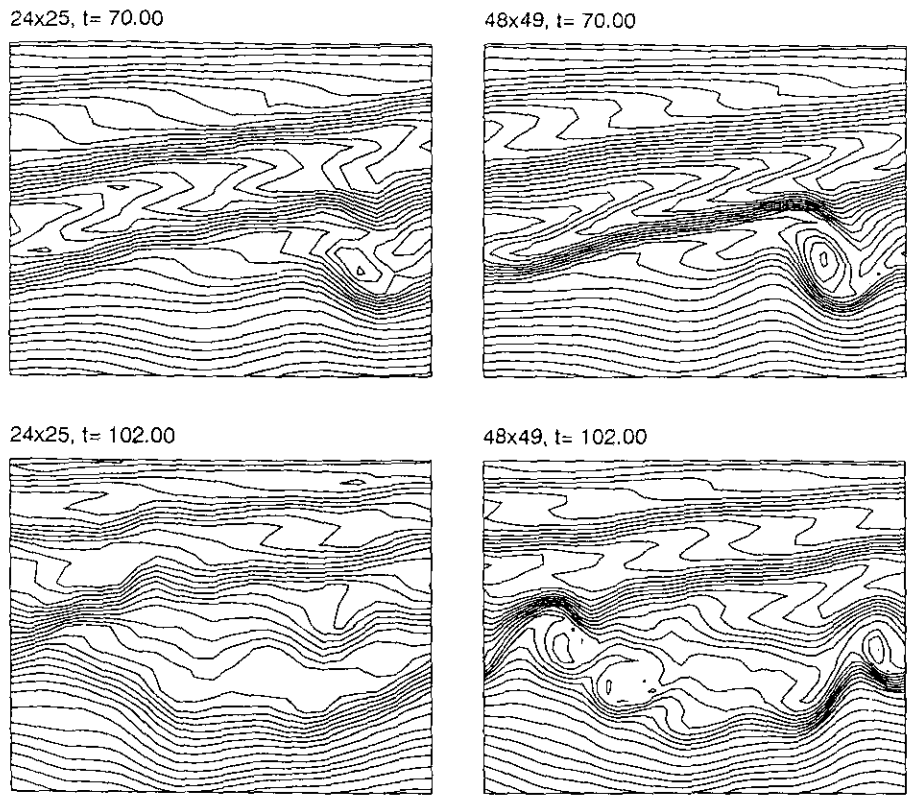

FIG. 15. Level curves for the logarithm of the potential temperature at $t = 70$ and $t = 102$ for 24×25 and 48×49 points. Spectral viscosity parameters (38b) (Case 2).

As mentioned in Section 4, the spectral viscosity terms (17) could be used instead of (18). With (17) and the parameters from Case 2 (where κ is no longer used and the same ε is used in all four equations), the results are very similar to the previous ones, both in terms of time-steps (see Fig. 13) and the solution itself. With the spectral viscosity terms (17), second derivatives of ρ and p instead of T must be calculated, but because the spectral representation of ρ and p already is calculated, the total number of transforms between physical and spectral space remains the same in our code. We believe that the terms (18), which are connected to the physics of the problem, is a good choice.

Numerical experiments mentioned in [23] indicated that the viscosity coefficients should vary smoothly from zero for $|k| < m_N$ to their values in the viscous part of the spectrum. Therefore viscosity coefficients of the form

$$\hat{Q}_k = \begin{cases} 0, & 0 \leqslant |k| \leqslant m_M, \\ \exp\left\{-\dfrac{(|k| - M/2)^2}{(|k| - m_M)^2}\right\}, & m_M < |k| \leqslant M/2, \end{cases} \tag{39a}$$

$$\hat{R}_l = \begin{cases} 0, & 0 \leqslant l \leqslant m_N, \\ \exp\left\{-\dfrac{(l - N/2)^2}{(l - m_N)^2}\right\}, & m_N < l \leqslant N, \end{cases} \tag{39b}$$

were tested. The coefficients (39) and parameters,

$$C_x = 1.0, \quad C_z = 2.0, \quad \varepsilon = 0.028, \quad \kappa = 0.00028, \tag{40}$$

give filters that are similar to those with (37) and the parameters from Case 2 (38b), but with more smooth functional forms. Again, as seen from the time-steps displayed in Fig. 13, the effects of this change were small. The numerical solution is slightly smoother with (39), (40), but it is difficult to judge which of the solution is the better.

Finally, to test the robustness of the method we used the set of parameters (38b), which was found by lots of experiments to be a good choice for 24×25 points, with different numbers of points. Time-steps for different numbers of points are shown in Fig. 14. The effect of the SV is, first, that the phase with stability-restricted time-steps is extended, and, second, that a second phase with stable or growing time-steps occurs, whereas the time-steps continue to drop in the inviscid cases. In this last part of the simulation the time-steps are accuracy-bounded and are therefore determined by the largest eigenvalue of the Jacobian of the ODE-system that has non-negligible amplitude, according to (26) and (27). It is natural that this eigenvalue (a) and the amplitude (U_n) of the corresponding solution component vary according to the dynamics of the system, leading to

some variations in the time-steps as the simulations proceed. From calculated mean values of the time-steps in this phase we estimate the time-steps to be $O(N^{-0.8})$. The fact that the time-steps for each simulation seem to end up in some limited interval indicate that the choices of parameters were successful. We can also see from Fig. 15, which shows the potential temperatures at $t = 70$ and $t = 102$ for 24×25 and 48×49 points, that the main features in the plots are the same, even though the coarse resolution in the first case limits the details that can be captured.

7. CONCLUSIONS

A physical situation occurring in simulation of waves in a stratified atmosphere has been used as a test problem for calculations with spectral methods. Straightforward spectral collocation simulation of the non-linear inviscid Euler equations suffers from unphysical oscillations in the numerical solution due to the absence of dissipation in the calculations and will eventually break down.

The spectral viscosity method has been applied to overcome this problem and seems to be a simple way to stabilize the calculations for long-time simulations. The spectral viscosity method involves some parameters which must be given appropriate values to obtain good results. These parameters decide the form and amplitude of the viscosity kernels, and to find good values for the parameters we have run a large number of low-resolution simulations. The results were evaluated by inspecting the numerical solution for the physical variables in terms of smoothness and correspondence with simulations with higher resolutions, by examining the spectra of the numerical solutions and by the measuring the time-steps chosen by an adaptive algorithm for the solution of the resulting system of ordinary differential equations.

The main results concerning the tuning of parameters were that a rather heavy damping of the highest frequencies were not sufficient and the pileup of energy occurred at lower frequencies instead. On the other hand, damping of a large part of the spectrum could also be insufficient if the amplitude was small or inefficient, in terms of time-steps for larger amplitudes. The best results were obtained when these situations were avoided, applying a viscosity kernel that started to act lightly on the frequencies below the highest crucial ones and growing to make stronger impact on the highest frequencies.

When the best set of parameters had been determined by these low-resolution experiments, the same values were used in simulations with higher resolution and were produced satisfying results. The theoretical basis for the spectral viscosity method incorporates the effects of changing the number of points, so a full new tuning of the parameters when the resolution is changed should be unnecessary.

The spectral viscosity method for expansions in Chebyshev polynomials has been subject to less work both in terms of analysis and numerical experiments than for Fourier or Legendre expansions, but the method is working well with the same amount of spectral viscosity applied in the Fourier and Chebyshev directions. The only additional concern is the role of the Chebyshev weight functions, where two alternatives have been tested in this work.

Regarding the time-step restrictions for the ODE-system resulting from the spectral viscosity method, we have found that the stability restriction for this system is left unchanged. The two main differences from the inviscid system for our model problem is first that the initial phase of stability-restricted time-steps lasts longer and second that the severe accuracy restrictions occurring later in the calculations are loosened, due to the reduced buildup of energy at high frequencies. Instead of reaching a point where the required accuracy can no longer be obtained, the simulation with spectral viscosity continues with time-steps within an interval determined by the level of detail that is possible to resolve with a given number of grid points. A result of this behaviour of the ODE-system is that the additional 50% computational work required by the SV method due to extra transforms between physical and spectral space, can be won back through larger time-steps for a large part of the simulation.

The method described in this paper has been successfully extended to do three-dimensional simulations of gravity wave/wind shear interactions, where 48 to 96 points are used in each direction. This will be described in a later paper.

ACKNOWLEDGMENTS

We thank Eitan Tadmor for his advice on the form of the Chebyshev SV terms and comments on a draft of this paper. Computer time on the CRAY at SINTEF in Trondheim were provided by the Norwegian Research Council for Science and the Humanities (NAVF).

REFERENCES

1. Ø. Andreassen, Numerical problems in gravity wave simulation, in *Proceedings, NATO Advanced Research Workshop on Coupling Processes in the Lower and Middle Atmosphere*, edited by E. V. Thrane *et al.*, NATO ARW Series (Kluwer Academic, Boston, 1993.)
2. M. Bjørhus, Technical Report FFI/RAPPORT-91/7011, Norwegian Defence Research Establishment, P.O. Box 25, N-2007 Kjeller, Norway, July 1991; *SIAM J. Sci. Stat. Comput.*, submitted.
3. W. Cai and C.-W. Shu, ICASE Report No. 91-26, NASA Langley Research Center, Hampton, Virginia 23665-5225, March 1991; *J. Comput. Phys.* **107**, 84 (1993).
4. C. Canuto, M. Y. Hussaini, A. Quarteroni, and T. A. Zang, *Spectral Methods in Fluid Dynamics* (Springer-Verlag, New York, 1988).
5. C. Canuto and A. Quarteroni, *J. Comput. Phys.* **71**, 100 (1987).
6. G. Erlebacher, M. Y. Hussaini, C. G. Speziale, and T. A. Zang, ICASE

Report No. 90-76, NASA Langley Research Center, Hampton, Virginia 23665-5225, October 1990; *J. Fluid Mech.*, to appear.

7. D. C. Fritts, *J. Atmos. Sci.* **35**, 397 (1978).
8. D. C. Fritts, *Pure Appl. Geophys.* **130**, 343 (1989).
9. D. Gottlieb and S. A. Orszag, *Numerical Analysis of Spectral Methods: Theory and Applications* (SIAM, Philadelphia, 1977).
10. E. Hairer, S. P. Nørsett, and G. Wanner, *Solving Ordinary Differential Equations I, Nonstiff Problems* (Springer-Verlag, New York, 1987).
11. T. Kato, *Perturbation Theory for Linear Operators* (Springer-Verlag, New York, 1986).
12. P. Lancaster and M. Tismenetsky, *The Theory of Matrices*, 2nd ed. (Academic Press, Orlando, FL, 1985).
13. L. D. Landau and E. M. Lifshitz, of *Course of Theoretical Physics.* Vol. 6. Fluid Mechanics. (Pergamon Press, London, 1959).
14. I. Lie, Technical Report FFI/Rapport-89/7017, Norwegian Defence Research Establishment, P.O. Box 25, N-2007 Kjeller, Norway, November 1989; *SIAM J. Sci. Stat. Comput.*, to appear.
15. Y. Maday, S. M. Ould Kaber, and E. Tadmor, Technical Report 91035, Laboratoire d'Analyse Numérique, Université Pierre et Marie Curie, Paris, France, 1991; *SIAM J. Numer. Anal.*, to appear.
16. Y. Maday and E. Tadmor, *SIAM J. Numer. Anal.* **26**, 854 (1989).
17. P. S. Marcus, "Numerical Modeling of Subgrid-Scale Flow in Turbulence, Rotation, and Convection," in *Astrophysical Radiation Hydrodynamics*, edited by K.-H. A. Winkler and M. L. Norman (Reidel, Dordrecht, 1986), p. 387.
18. P. Moin, K. Squires, W. Cabot, and S. Lee, *Phys. Fluids A* **3**(11), 2746 (1991).
19. S. Schochet, *SIAM J. Numer. Anal.* **27**, 1142 (1990).
20. E. Tadmor, private communication.
21. E. Tadmor, ICASE Report No. 88-41, NASA Langley Research Center, Hampton, Virginia 23665-5225, July 1988 (unpublished).
22. E. Tadmor, *SIAM J. Numer. Anal.* **26**, 30 (1989).
23. E. Tadmor, "Shock Capturing by the Spectral Viscosity Method," in *Spectral and High Order Methods for Partial Differential Equations*, edited by C. Canuto and A. Quarteroni (North-Holland, Amsterdam, 1990), p. 197; *Comput. Methods Appl. Mech. Eng.* **80** (1990).
24. C. E. Wasberg and Ø. Andreassen, "Pseudospectral Methods with Open Boundary Conditions for the Study of Atmospheric Wave Phenomena," in *Spectral and High Order Methods for Partial Differential Equations*, edited by C. Canuto and A. Quarteroni (North-Holland, Amsterdam, 1990), p. 459; *Comput. Methods Appl. Mech. Eng.* **80** (1990).